Preparation of biodegradable polymeric nanoparticles for pharmaceutical applications using glass capillary microfluidics

Rahimah Othman[a,c*], Goran T. Vladisavljević[a*], Zoltan K. Nagy[a,b]

[a]*Department of Chemical Engineering, Loughborough University, Ashby Road, Loughborough, Leicestershire LE11 3TU, UK.*

[b]*School of Chemical Engineering, Purdue University, West Lafayette, IN 47907-2100, USA.*

[c]*School of Bioprocess Engineering, Universiti Malaysia Perlis, Kompleks Pusat Pengajian Jejawi 3, 02600 Arau, Perlis, Malaysia.*

**Corresponding authors: Email R.Othman@lboro.ac.uk, G.Vladisavljevic@lboro.ac.uk*

ABSTRACT

The aim of this study was to develop a new microfluidic approach for the preparation of nanoparticles with tuneable sizes based on micromixing / direct nanoprecipitation in a coaxial assembly of tapered-end glass capillaries. The organic phase was 1 wt% poly(ε-caprolactone) (PCL) or poly(dl-lactic acid) (PLA) in tetrahydrofuran and the antisolvent was Milli-Q water. The size of nanoparticles was precisely controlled over a range of 190-650 nm by controlling phase flow rates, orifice size and flow configuration (two-phase co-flow or countercurrent flow focusing). Smaller particles were produced in a flow focusing device, because the organic phase stream was significantly narrower than the orifice and remained narrow for a longer distance downstream of the orifice. The mean size of PCL particles produced in a flow focusing device with an orifice size of 200 μm, an organic phase flow rate of 1.7 mL h^{-1} and an aqueous-to-organic flow rate ratio of 10 was below 200 nm. The size of nanoparticles decreased with decreasing the orifice size and increasing the aqueous-to-organic phase flow rate ratio. Due to

higher affinity for water and amorphous structure, PLA nanoparticles were smaller and exhibited a smoother surface and more rounded shape than PCL particles.

Keywords: Biodegradable nanoparticles; Nanoprecipitation; Microfluidic micromixing; Poly(ε-caprolactone); Poly(dl-lactic acid); Glass capillary devices.

1. Introduction

Biodegradable polymeric nanoparticles (NPs) have attracted considerable attention of the scientific community in the last several decades due to their high potential for a site-specific (targeted) drug delivery, especially for oral administration of proteins and peptides and gene therapy (Legrand et al., 2007; Douglas et al., 1987). Biodegradable polymeric NPs are solid carriers with a mean size of less than 1 μm, which are capable to dissolve, entrap, encapsulate or attach active ingredients to its nanoparticle matrix (Legrand et al., 2007). Depending upon the method of NPs preparation and formulation, nanospheres or nanocapsules can be obtained. Nanocapsules are carriers in which the drug is confined to a cavity surrounded by a polymeric shell, while nanospheres are matrix systems in which the drug is uniformly dispersed in a polymer matrix (Mohanraj and Chen, 2007; Soppimath et al., 2001).

Polymeric NPs can be prepared from preformed polymers by emulsification-solvent evaporation, salting-out, dialysis, nanoprecipitation, and supercritical fluid technology or directly synthesised by polymerisation of monomers using polymerisation techniques such as micro-emulsion, mini-emulsion, surfactant-free emulsion and interfacial polymerisation (Nagavarma et al., 2012; Rao and Geckeler, 2011; Galindo-Rodriguez et al., 2004). In nanoprecipitation, two mutually miscible liquids are required, a solvent and non-solvent of the polymer, typically a volatile organic solvent and water, respectively. The NPs are formed almost instantly when the

polymer solution is mixed with an excess of non-solvent, after which the solvent can be evaporated off. The method does not require high stirring rates, sonication, elevated temperatures or surfactants, and Class 1 solvents can be avoided (Fessi et al., 1989, 1992; Jain, 2000).

Bilati et al. (2005) have investigated the effect of the type of solvent and non-solvent, solvent/non-solvent volume ratio and polymer concentration on the nanoprecipitation of polylactide (PLA) and poly(d,l-lactic-*co*-glycolic acid) (PLGA). The size of NPs was dependent of the type of non-solvent and increased in the following order: methanol < ethanol < propanol. Lince et al. (2008) prepared poly-ε-caprolactone (PCL) nanoparticles in a Confined Impinging Jets Reactor (CIJR) and found a significant effect of mixing on the final particle size. The mixing efficiency increased with increasing the flow rate of the liquid phases entering the CIJR, which favoured nucleation and led to a marked reduction in the particle size.

In order to achieve a controlled drug release to the specific site of action at the therapeutically optimal rate, NPs should be prepared with a controlled size, adhesion properties and degradation rate (Mohanraj and Chen 2007). The traditional bulk mixers lack precise control over the mixing process due to their relatively large volume, resulting in poor control over the particle size distribution. Microscale mixers/reactors handle very small fluid volumes, offering the possibility to achieve a homogeneous reaction environment, and have a larger surface-to-volume ratio than conventional bulk mixers, which can greatly reduce the mixing time that becomes comparable with the induction time for nucleation (Capretto et al., 2013).

Ali et al. (2009) prepared hydrocortisone NPs in a microfluidic Y junction. The size of the generated NPs was controlled by the flow rates of solvent and anti-solvent, with smaller particles being formed at higher flow rates. Su et al. (2007) prepared $BaSO_4$ and 2,2-dipyridylamine NPs using a microfluidic set-up composed of three T-junctions. Solvent and anti-solvent droplets

were formed in two upstream T junctions and then merged together in a downstream T junction. Génot et al. (2010) positioned a glass capillary at the intersection of the two branches of a Y junction to construct a 3D microfluidic mixer that was used to prepare rubrene nanocrystals. Zhang et al. (2008) and Yun et al. (2009) produced solid lipid nanoparticles using flow focusing devices with cross junction geometry. The particle size was controlled by varying the flow rate ratio of the two phases and introducing gas bubbles downstream of the cross junction. Dev et al. (2013, 2012) used a microfluidic continuous flow rotating tube processor to produce NPs of meloxicam and curcumin by reactive crystallisation.

Membrane micromixing is an alternative strategy of controlled mixing at molecular scale that was combined with nanoprecipitation to produce inorganic nanoparticles (Jia and Liu, 2013), liposomes (Laouini et al., 2013a), micelles (Laouini et al. (2013c), and PCL nanoparticles (Khayata et al., 2012). In a membrane-dispersion reactor, one liquid phase is dispersed through a microporous membrane into another liquid under controlled shear conditions and injection rate.

In this work, a novel microfluidic strategy was developed for fabrication of PCL and PLA NPs based on bringing into contact two co-flowing or counter-current flowing streams in coaxial glass capillaries. Both polymers have been approved by FDA for drug delivery (Jain et al., 1998; Södergård and Stolt, 2002; Panyam and Labhasetwar, 2003) and widely used as excipients in nanoprecipitation processes (Jain, 2000; Lu and Chen, 2004). The main objectives of this study were: (i) to make appropriate choice of good and poor solvent of the polymers, (ii) to observe the mixing process *in situ* using a microscope video system, and (iii) to investigate the effect of operating parameters, system geometry, and surfactants on the final particle size distribution.

2. Materials and Methods

2.1. Chemicals

Tetrahydrofuran (THF) (HPLC grade, purity ≥ 99.9%) and poly(ε-caprolactone) (PCL, M_w = 14,000 g mol^{-1} with a glass transition temperature of 60 ^oC) were purchased from Sigma-Aldrich (Dorset, UK). Poly(dl-lactic acid) (PLA, Ingeo^{TM} 4060D, M_w = 320,000 g mol^{-1}) was supplied by Natureworks LLC (Minetonka, MN, USA). 4060D is an amorphous polymer with an average D-lactide content of 12 wt% and a glass transition temperature of 55-60^oC. Polyvinyl alcohol (PVA), polyvinyl pyrrolidone (PVP), Tween 20, and Tween 80 were obtained from Sigma-Aldrich (Dorset, UK) and used as water soluble surfactants. All chemicals other than THF were of analytical grade. The antisolvent phase was pure water produced by reverse osmosis (Milli-Q®, Millipore) or aqueous surfactant solutions. The role of surfactant was to prevent agglomeration, coalescence and imperfect surface formation, as well as to reduce the size of the NPs. The organic phase was a homogeneous solution containing 1 g L^{-1} (1000 ppm) of the polymer (PCL or PLA) in THF.

2.2. Equipment

The experiments have been carried out using two different types of glass capillary devices shown in Figs. 1 (b) and (c). The main body of the device was made up of two coaxial glass capillaries: an inner capillary with a circular cross section (1 mm O.D. and 0.58 mm I.D.) and an outer capillary with a square cross section (1 mm I.D.). A two-component epoxy glue (Five Minute® Epoxy, ITW Devcon, Rushden, UK) was used to fix the square capillary onto a glass microscope slide that was used as a platform for the microfluidic device. One end of the inner capillary was shaped into a tapered orifice with an I.D. of 60, 150, 200, 300 or 400 μm. It was done by heating and pulling the capillary using a Sutter P-97 Flaming/Brown micropipette puller

(Linton Instrumentation, Norfolk, UK) to produce a sharp tip with 20 μm orifice. The diameter of the orifice was then enlarged by grazing the tip against abrasive paper until the required size was achieved and the orifice had a smooth edge, which was observed with a Narishige's MF-830 microforge (Linton Instrumentation, Norfolk, UK). The capillary was then treated with 2-[methoxy(polyethyleneoxy)propyl]trimethoxysilane (FluoroChem, UK) to enhance the hydrophilicity of the orifice. After subsequent cleaning and treatment, the round capillary was positioned inside the square capillary such that the orifice coincides with the longitudinal axis of the square capillary. Two syringe needles (2.5 mm O.D. and 0.9 mm I.D.) with plastic hubs (B-D Precisionglide®, Sigma-Aldrich, Dorset, UK) were glued onto the slide such that the entrances to each capillary were situated inside the hubs.

2.3. Experimental set-up and preparation of polymeric NPs

Two 11 Elite syringe pumps (Harvard Apparatus, Cambridge, UK) were used to deliver the organic and aqueous phase from SGE syringes to their respective capillaries. In a co-flow device (Fig. 1b), the organic phase was delivered to the inner capillary, the aqueous phase flowed co-currently through the space between the square and inner capillary and the product suspension exited through the square capillary. In a flow focusing device (Fig. 1c), the organic phase was delivered to the outer capillary, the aqueous phase flowed counter-currently through the space between the two capillaries and the product suspension was collected from the inner capillary. Teflon (PTFE) tubing (1.59 mm O.D. and 0.8 mm I.D.) resistant to THF was used to deliver the organic phase and polyethylene tubing (1.52 mm O.D. and 0.86 mm I.D.) was used for the aqueous phase.

NPs were formed downstream of the orifice when both streams were brought into contact. This was observed through an inverted microscope and recorded by a Phantom V9.0 high-speed

camera (Vision Research, Ametek, US) at 25 frames per second with 576 × 288 resolution. The flow rates of the two phases and the orifice diameter were systematically varied in order to study their effects on the average size of the NPs and their particle size distribution. The fresh nanosuspension was collected in a vial via PTFE tubing (1.5 mm I.D.), after which the organic solvent was completely evaporated in a vacuum oven (Technico, Fistreem International Ltd, Loughborough, UK) under absolute pressures below 10 torr and the room temperature for about 30 min until the smell of THF had disappeared completely.

2.4. Characterisation of nanoparticles

2.4.1. Particle size analysis

The size distribution of NPs was determined by dynamic light scattering (DLS) using Delsa™ Nano HC Particle Analyzer (Beckman Coulter, High Wycombe, UK), which measures the fluctuations of scattered light as a function of time. NPs were diluted 5-fold by Milli-Q water before being transferred into a 4 mL disposable cuvette which was then placed into the instrument. The measurement time was 120 s. The measurements were repeated thrice at a scattering angle of 165° and a temperature of 25 °C using CONTIN and Cumulants methods. The Cumulants method provides a *z*-average value (the harmonic intensity-weighted average diameter of the particles) and a polydisperity index (PDI), a "dimensionless measure of the broadness of the size distribution" as defined by the British Standard (BSI, 1997). CONTIN algorithm provides average peak diameter values from intensity distribution (British Standards Institution, 1997).

2.4.2. Zeta potential determination

The zeta potential of NPs was measured by electrophoretic light scattering (Laser Doppler electrophoresis) using a Delsa™ Nano HC Particle Analyzer (Beckman Coulter, High Wycombe,

UK). The measurements were repeated three times after sample dilution with Milli-Q water. The zeta potential was calculated from the electrophoretic mobility using the Helmholtz-Smoluchowski equation (Submicron, 2011).

2.4.3. Microscopic observations (TEM and FEGSEM)

The internal structure and surface morphology of the NPs was investigated using Transmission Electron Microscopy (TEM) and high resolution Field Emission Gun Scanning Electron Microscopy (FEG-SEM). For TEM analysis, a sample drop was deposited onto a carbon-coated copper mesh and left to dry before being observed by a JEOL JEM-2000 FX transmission electron microscope operated at an accelerating voltage of 200 kV. The mesh was coated by dipping it into a suspension of carbon particles in deionised water.

FEG-SEM images were obtained using a LEO 1530 VP (LEO Elektronenmikroskopie GmbH, Oberkochen, Germany) scanning electron microscope with an integrated EDAX TEAM™ Pegasus EBSD/EDXA (electron backscatter diffraction/energy dispersive x-ray analysis) system. FEG-SEM has the advantage over conventional SEM of providing higher resolution images due to a smaller diameter of the electron beam, which gives a higher signal to noise ratio leading to improved spatial resolution. The samples were placed onto conventional aluminium sample holders with a diameter of ~1 cm. For NPs imaging, the chamber was evacuated to ~0.5 Pa and the images were taken using in-lens detector operating at an accelerating voltage of 5-10 keV and a working distance of 5-10 mm.

3. Results and Discussion

3.1. Prediction of solvent-water interactions

The choice of organic solvent is a crucial initial step that should be taken. The organic solvent must be able to dissolve polymer and must be miscible with water, which can be estimated using the combined solubility parameter (Van Krevelen and Hoftyzer, 1976):

$$\Delta\delta_{solvent-water} = [(\delta_{d,S} - \delta_{d,W})^2 + (\delta_{p,S} - \delta_{p,W})^2 + (\delta_{h,S} - \delta_{h,W})^2]^{1/2} \quad (1)$$

where δ_d is the dispersion solubility parameter due to London dispersion forces resulting from the existence of induced dipoles as two molecules approach each other, δ_p is the polar solubility parameter due to Keesom forces occurring when two permanent dipoles are present, and δ_h is the hydrogen bonding solubility parameter (Bordes et al., 2010; Hansen, 2007). The subscripts *S* and *W* refer to the organic solvent and water, respectively. Table 1 lists the combined solubility parameters of six potential volatile organic solvents: acetone (Ac), tetrahydrofuran (THF), ethanol (EtOH), dimethyl sulfoxide (DMSO), isopropyl alcohol (IPA) and ethyl lactate (EL), calculated from Eq. (1) using the partial solubility parameters from Table 1. The value of $\Delta\delta_{solvent-water}$ increases in the following order: EtOH < DMSO < IPA < EL < Ac < THF. The smaller the $\Delta\delta_{solvent-water}$ value, the higher the affinity of solvent for water and the higher its solubility into the aqueous phase, hence smaller NPs can be produced.

Solvent toxicity is another important aspect for pharmaceutical applications. All solvents in Table 1 except THF are categorized as class 3 by the U.S. Food and Drug Administration (FDA). The former permissible daily exposure (PDE) for THF was 121 mg/day and THF was categorized as class 3 solvent. Based on new toxicological data, the PDE for THF is 7.2 mg/day, and the new FDA's recommendation is to move THF from class 3 to class 2.

To completely explain the behaviour of solvent in nanoprecipitation process, the solvent-water interaction parameter must also be considered (Martin et al., 1993):

$$\chi_{solvent-water} = \frac{V_{solvent}}{RT}(\delta_{solvent} - \delta_{water})^2 \quad (2)$$

where $V_{solvent}$ is the molar volume of the solvent, R is the universal gas constant (8314 J kmol^{-1} K^{-1}), T is the absolute temperature, and $\delta_{solvent}$ and δ_{water} are the total solubility parameters of the solvent and water, respectively, provided in Table 1. The values of $\chi_{solvent-water}$ calculated using Eq. (2) increase in the following order: EtOH < DMSO < IPA < Ac < THF < EL. Solvents that have a high affinity for water, which is evidenced by low $\chi_{solvent-water}$ values, tend to promote solvent diffusion and polymer partition into the aqueous phase, which leads to the formation of smaller NPs (Legrand et al., 2007; Galindo-Rodriguez et al., 2004). $\Delta\delta_{solvent-water}$ and $\chi_{solvent-water}$ in Table 1 are in good correlation with each other, indicating that EtOH, DMSO and IPA have the highest affinity for water. On the other hand, Ac, THF and EL show a relatively low affinity for water, either due to their low polarity (e.g. THF), or low hydrogen-bonding preference (Ac) or several combined factors (EL). In addition to solvent-water interactions, the polymer interactions with solvent and water must also be considered.

3.2. Prediction of polymer-solvent and polymer-water interactions

The extent of polymer-solvent interaction can be estimated from a 2-D graph (Bagley et al., 1971), in which a hydrogen bonding solubility parameter, δ_h is plotted against Bagley's two-dimensional solubility parameter, δ_v, where $\delta_v = (\delta_p^2 + \delta_d^2)^{1/2}$. The good solvents are those that are included within a circle of a radius of five δ-units around the polymer (Van Krevelen and

Hoftyzer, 1976; Choi et al., 2002; Su et al., 2007). Fig. 2 shows a Bagley's two-dimensional solubility graph for two polymers (PLA and PCL), water and six organic solvents. The centre of the solubility circle of PLA corresponds to values of δ_h and δ_v in Table 1 listed under the heading PLA[a], calculated based on the classical method for Hansen solubility parameters (Van Krevelen and Hoftyzer, 1976). As expected, water appears far outside the solubility circle of PLA and PCL, in agreement with the fact that it is a nonsolvent of these polymers. IPA and EtOH are also outside the both solubility circles, due to high δ_h values as a result of extensive hydrogen bonding between their molecules. Therefore, both solvents are bad solvents for PLA and PCL, but with the highest affinity for water among all the solvents studied. The solubility graph also suggests that acetone is a bad solvent for PLA, whereas DMSO is a bad solvent for PCL. Thus, only THF and EL are good solvents for both polymers and suitable for the formation of PLA and PCL NPs. In a good solvent, polymer chains are more disentangled from one another and extensively solvated. Conversely, in a poor solvent, polymer chains are more shrunken and their solvation is limited (Galindo-Rodriguez et al., 2004).

The solubility of PLA and PCL in the investigated solvents can also be predicted using the Hansen sphere space theory. The distance between a solvent (*S*) and the polymer (*P*) in the "$2\delta_d$ - δ_p - δ_h solubility space" is given by:

$$D = [4(\delta_{d,S} - \delta_{d,P})^2 + (\delta_{p,S} - \delta_{p,P})^2 + (\delta_{h,S} - \delta_{h,P})^2]^{1/2} \quad (3)$$

The D values for six selected organic solvents calculated from Eq. (3) are shown in Table 2. Good solvents for the given polymer lie within the solubility sphere of radius R_0, known as the interaction radius. The interaction radius for PCL with M_w = 14,000 g mol^{-1} is 7.1 (Bordes et al., 2010). From Table 2, EtOH, IPA and DMSO are nonsolvents for PCL ($D > 7.1$), which

agrees with the predictions from Fig. 2. The interaction radius for PLA at 25°C is 6.4 (Hansen, 2007), which means that EtOH, IPA, Ac, and DMSO can be regarded as nonsolvents for PLA.

Polymer-water compatibility can be predicted from the combined polymer-water solubility parameter, $\Delta\delta_{polymer-water}$: for a good compatibility, $\Delta\delta_{polymer-water}$ must have a small value (Van Krevelen and Hoftyzer, 1976). The values of $\Delta\delta_{polymer-water}$ in Table 1 increase in the following order: PLA[a] < PLA[b] < PCL. Clearly, PLA shows higher compatibility with water, because PLA is more polar than PCL ($\delta_{p,PLA}$ = 9.7 and $\delta_{p,PCL}$ = 4.8). The polarity of PLA and PCL originates from their ester bonds, but PCL has a longer nonpolar hydrocarbon chain between ester linkages, [–$(CH_2)_5$–], as compared to PLA, [–$CH(CH_3)$–].

The combined polymer-solvent solubility parameters are shown in Table 3. For PLA[a], the $\Delta\delta_{polymer-solvent}$ values increase as follows: EL < Ac < THF < IPA < DMSO < EtOH. Therefore, THF, Ac and EL show the highest compatibility with both polymers. The solvent-polymer Flory-Huggins interaction parameter, $\chi_{solvent-polymer}$ is another measure of the interaction between polymer chains and solvent molecules and can be calculated as (Hansen, 2007):

$$\chi_{solvent-polymer} = \frac{V_{solvent}}{RT}[(\delta_{d,S} - \delta_{d,P})^2 + (\delta_{p,S} - \delta_{p,P})^2 + (\delta_{h,S} - \delta_{h,P})^2] \quad (4)$$

The values of $\chi_{solvent-polymer}$ for six different solvents are summarised in Table 3. For $\chi_{solvent-polymer}$ < 0.5, the polymer is soluble in a solvent over entire concentration range (Bordes et al. (2010) and if $\chi_{solvent-polymer}$ > 0.5, the polymer is hardly soluble or insoluble. The results in Fig. 2 and Table 3 partially contradict each other, since Table 3 implies that only EL is a good solvent for PLA[a], while Fig. 2 suggests that THF, EL, and DMSO are all good solvents for PLA[a]. It may be attributed to large variations in PLA solubility depending on the degree of crystallinity, which is

determined by the ratio of D to L enantiomers. In this work, THF will be used as a solvent for PLA, since a 50:50 mixture of the D and L enantiomers is amorphous and soluble in THF, contrary to pure D or L forms. In addition, THF has a boiling point of 66^{o}C, which is much lower than the boiling point of EL of 151^{o}C and therefore, can be readily removed from the suspension through vacuum evaporation.

3.3. Effect of organic solvent removal

The average particle size, Z_{ave} and the polydispersity index, *PDI* in the samples prepared in a co-flow device were measured in fresh nanosuspensions and the samples stored in a vacuum evaporator (Table 4). Due to evaporation of residual THF from PCL particles, the particle diameter decreased 11-14 % of its original size, which is equivalent to the volumetric shrinkage of 28-37 %. After nanoprecipitation, THF is redistributed between the liquid phase and NPs until equilibrium is reached characterized by equal chemical potential of THF in both phases. Since $\Delta\delta_{PCL-THF}$ « $\Delta\delta_{THF-water}$ ($\Delta\delta_{PCL-THF}$ =1.00 and $\Delta\delta_{THF-water}$=36.91 J$^{1/2}$cm$^{-3/2}$ from Tables 1 and 3), THF is much more compatible with PCL than water. As a result, the content of THF in the liquid phase immediately after PCL precipitation is 9.1 vol%, while its content in the swollen NPs is about 28-36 vol%. However, due to very small volume fraction of NPs of about 10^{-4}, more than 99.9 vol% of THF added to the system is present in the liquid phase, and less than 0.01 vol% is absorbed within the swollen NPs. As THF evaporates, its concentration in the aqueous phase decreases, which causes a decrease in the chemical potential of THF in the liquid phase and further diffusion of THF to the liquid phase until the equilibrium is reestablished. The process of THF dissolution continues until virtually all THF is removed from the NPs. The shrinkage percentage was independent on the initial particle size, which means that THF was completely removed from the particles in all cases. In all subsequent experiments, THF was completely

removed from the NPs before analysis. The PDI values for the fresh samples were in the range of 0.178-0.219 (Table 4). After solvent evaporation, the samples were significantly concentrated with a higher agglomeration tendency, which led to increased PDI values (0.219-0.294).

3.4. Effects of aqueous-to-organic flow rate ratio, orifice size and polymer type

3.4.1. Constant aqueous phase flow rate and variable organic phase flow rate

In these experiments in a co-flow device, Q_{aq} was kept constant at 5 mL h^{-1} and Q_{or} ranged from 3.3 to 0.5 mL h^{-1} corresponding to Q_{aq}/Q_{or} ratio from 1.5 to 10, respectively. The size of NPs was found to decrease with increasing Q_{aq}/Q_{or}, as shown in Fig. 3. At higher Q_{aq}/Q_{or} ratio, the particle nuclei are more diluted after formation, which suppresses the rate of particle growth given by: $dl/dt = K_g(C_i - C^*)^b$, where K_g is the particle growth rate constant and C_i and C^* are the polymer concentration on the particle surface and the saturation concentration, respectively. The value of the parameter b is usually between 1 and 3 (Zhao et al., 2007). The increased water flow rate decreases the polymer concentration on the particle surface, C_i, leading to a decrease in $C_i - C^*$ and the rate of particle growth, thereby resulting in smaller ultimate particle size. The increased water volume also decreases the tendency for particle aggregation due to lower frequency at which particles collide with and stick to each other. The particle aggregation is most likely near the orifice, where the local particle concentrations are high. In addition, a higher flow rate ratio provides a more rapid mixing in a microfluidic system (Génot et al., 2010). In a more rapid mixing process, the critical supersaturation needed for nucleation is reached faster, which allows for the generation of more nuclei, whose growth will

be limited by the amount of available polymer in the liquid phase. Therefore, a larger number of nuclei will lead to smaller size of NPs. The smaller particle sizes at higher aqueous-to-organic volume ratios were also obtained by Laouini et al. (2013a, 2013b, 2013c) in the production of liposomes and polymeric micelles in membrane contactors and by Jahn et al. (2010) in the formation of liposomes in planar flow focusing microfluidic mixers.

At constant Q_{aq}/Q_{or} ratio, the particle size was found to significantly increase with increasing the orifice size, D_o over the range of 200-400 μm (Fig. 3). The mixing process is more efficient if the organic phase is injected through smaller orifice, due to greater shear stresses in the mixing zone and higher interfacial area per unit volume of the organic phase. At Q_{aq}/Q_{or}=1.5 and D_o=60 μm, the velocity of organic stream in the orifice is 0.324 m s^{-1} and the velocity of the surrounding aqueous phase is 1.4×10^{-3} m s^{-1}. However, at Q_{aq}/Q_{or}=1.5 and D_o =400 μm, the organic phase velocity in the orifice is only 7.3×10^{-3} m s^{-1} and the aqueous phase velocity is 1.6×10^{-3} m s^{-1}. Due to small difference in velocity between the two streams, the mixing process is less efficient leading to higher particle size. At D_o = 60 μm, the particle size was somewhat larger than that at 200 μm, which may be due to susceptibility of 60-μm orifice to particle deposition and clogging, which may compromise the particle size.

The micrographs of mixing zone in the device with a 60-μm orifice size at various flow rate ratios are shown in Fig. 4. At Q_{aq}/Q_{or}=10 (Fig. 4a and Video 1), the interface is spherical and resembles a familiar shape which can be seen when one immiscible liquid is introduced into another in the dripping regime (Vladisavljević et al., 2012). It is hard to explain this shape without acknowledging some type of interfacial tension, although THF and water are miscible in all proportions and should have zero equilibrium interfacial tension. In fact, when two miscible

fluids are suddenly put into contact, gradients of composition and density at the boundary can give rise to tension between the contacted fluids, which is known as the transient interfacial tension or Korteweg stress (Joseph and Venkatachalappa, 1999), given by:

$$\sigma = k\Delta C^2 / \delta \quad (5)$$

where k is the proportionality constant, ΔC is the change in concentration over the transition zone between two miscible fluids and δ is the thickness of the transition zone. The transient tension decreases rapidly during the process of dissolution in proportion to $\sqrt{D/t}$, where D is the diffusion coefficient and t is the interfacial age. At each Q_{aq}/Q_{or} value, there is a certain equilibrium size of a droplet formed at the capillary tip. At equilibrium, the rate of diffusion of the organic phase from the interface, due to mutual mixing at the contact zone, is equal to the rate of convective flow from the orifice toward the interface. The produced NPs form dark concentric layers around the interface, due to capillary waves (Fig. 4a). At Q_{aq}/Q_{or}=4.5 (Fig. 4b), the organic phase forms a widening jet due to increased inertial force that overcomes the transient interfacial tension and elongates the interface. The organic phase velocity at the orifice, U_{or} = 0.32 m s^{-1}, is much higher than the aqueous phase velocity, U_{aq} = 1.4 × 10^{-3} m s^{-1}, leading to deceleration of the organic phase in the direction of flow and causing widening of the jet. With further increase in velocity of the organic phase, a flow instability phenomenon known as "viscous fingering" occurs (Fig. 4c), which leads to distortion of the interface and formation of finger-like patterns. Such instability occurs typically when a less viscous fluid is injected into a more viscous one (it should be noted that the viscosity of THF at 293 K is 0.63 mPa s and the water viscosity is 0.99 mPa s). The penetration of the less viscous fluid is not uniform since part of the more viscous fluid forms fjords, named "viscous fingers" (Homsy, 1987). Viscous fingering was not observed when ethanolic solution of phospholipids was injected into water in

the same type of capillary device (Vladisavljević et al., 2014), because the viscosity of ethanol of 1.25 mPa s was higher than the water viscosity. At Q_{aq}/Q_{or} = 1.5, two symmetrical vortices were formed at the lower and upper parts of the capillary tube (Fig. 4d), due to high shear stress at the interface, caused by high difference in velocity between the organic and aqueous phase.

The particle size distribution curves at D_o =150 and 200 μm are in good agreement with the above observations featuring the minimum particle size at the maximum flow rate ratio (Fig. 5), due to shortest mixing time. The growth of nuclei is more limited if the mixing process is faster, which will lead to smaller NPs. At Q_{aq}/Q_{or} = 10, the mixing time is shortest due to the smallest amount of injected organic phase relative to aqueous phase. As a result, the interface disappears at the distance of just $4.4D_o$ downstream of the nozzle (Fig. 4a) and the NPs have the minimum size. At Q_{aq}/Q_{or} = 1.5, the mixing time is long due to high amount of injected organic phase. In addition, as a result of vortex flow, the nuclei formed near the nozzle are forced into circular motion, which can lead to their much longer residence time compared to the nuclei formed more downstream. As a consequence, the particle size distribution is very broad, as shown in Fig. 5a.

The effect of polymer type on the size of NPs at the orifice size of 60 μm is shown in Fig. 6a. PLA formed smaller particles than PCL, because PLA is more compatible with water, as can be seen by the lower $\Delta\delta_{polymer-water}$ value in Table 1. As a result, precipitation of PLA starts when the water content in THF reaches 31 vol%, while PCL starts precipitating out when the water content in THF is about 16 vol%. Therefore, PLA starts to precipitate from a more diluted polymer solution, which limits particle growth and leads to smaller particle size.

3.4.2. Constant organic phase flow rate and variable aqueous flow rate

In this set of experiments, the organic phase flow rate was kept constant at 1.7 mL h^{-1} and the aqueous phase flow rate varied from 2.55 to 17 mL h^{-1}, corresponding to Q_{aq}/Q_{or} value from 1.5 to 10 respectively (Fig. 6 b-d). At the same Q_{aq}/Q_{or} value, the particle size was smaller when the organic phase flow rate was maintained at 1.7 mL h^{-1} compared to the fixed aqueous phase flow rate of 5 mL h^{-1}. At Q_{or} = 1.7 mL h^{-1}, the total flow rate, $Q_{aq}+Q_{or}$ was in the range of 4.25-18.7 mL h^{-1}, whereas at Q_{aq} = 5 mL h^{-1}, the total flow rate was 5.5-8.3 mL h^{-1}. Probably, the mixing efficiency is higher at the higher flow rate in the collection capillary. Triple runs were carried out on each experiment to check reproducibility of the particle sizes and only small within-runs variations were observed, as indicated by small error bars. The opposite results were obtained by Jahn et al. (2010) in microfluidic preparation of liposomes, with smaller vesicle sizes obtained at smaller total flow rates. The minimum size of both PLA and PCL particles in a co-flow device was less than 250 nm and was achieved at Q_{aq}/Q_{or}=10 and for a 60-μm orifice size.

3.5. Co-current flow versus counter-current flow focusing

Micromixing in a glass capillary device has also been achieved by countercurrent flow focusing. The micrographs of the mixing zone of the device with an orifice size of 400 μm at Q_{or} = 1.7 mL h^{-1} and variable aqueous phase flow rate are shown in Fig. 7. Due to high velocity of aqueous phase, the jetting regime occurs at all flow rate ratios with very long widening jets and no signs of interfacial instability. The phase boundary is sharp at Q_{aq}/Q_{or} = 10 and 7, becomes blurred at Q_{aq}/Q_{or} = 4.5 and almost completely disappears at Q_{aq}/Q_{or} = 3. A sharp interface occurs due to sharp concentration gradients at the contact zone resulting from high

velocity of aqueous phase in the tapered section of the inner capillary. At Q_{aq}/Q_{or}=3, $\Delta C/\delta \approx 0$ due to relatively long residence time of liquid elements and mutual mixing of THF and water upstream of the orifice and $\sigma \approx 0$; thus, the phase boundary is hardly visible. At Q_{aq}/Q_{or} = 1.5, the phase boundary is invisible (the image not shown here). The dark areas in Fig. 7 are the regions within the device where the NPs are formed at relatively high concentration. These regions are mainly contact zones between the two phases upstream of the orifice where the fluid velocities are relatively small due to large cross-sectional area available for flow.

Fig. 8 provides a comparison of the average particle size, Z_{ave} in a co-flow and flow focusing device for the same flow rates and device geometry. Triple runs were carried out on each sample and small error bars in the graph indicate high reproducibility. The mixing time in a microfluidic flow focusing device is given by (Karnik et al., 2008): $\tau_{mix} \propto d_{or}^2/D$, where d_{or} is the diameter of the organic phase stream and D is the diffusivity of the solvent. The organic phase stream is wider at smaller Q_{aq}/Q_{or} (Fig. 7), which results in longer mixing times and larger Z_{ave} value (Fig. 8). The smaller NPs were produced in a flow focusing device compared to co-flow device of the same orifice size, which was most pronounced at the orifice size of 400 μm. In a flow focusing device, the diameter of the organic phase stream in the mixing zone is significantly smaller than the orifice diameter ($d_{or} \ll D_o$), while in a co-flow device the diameter of the organic phase stream corresponds to the orifice diameter ($d_{or} \approx D_o$). Therefore, under the same other conditions, τ_{mix} in flow focusing device is much smaller than that in a co-flow device. At D_o = 60 μm, there was no difference in performance between a co-flow and flow focusing microfluidic mixer. The orifice is prone to clogging in a flow focusing device by the

particles formed upstream of the orifice, which can be deposited onto the inner walls of the collection capillary as they pass through the orifice. Therefore, the optimum diameter of the orifice in flow focusing device was about 200 μm.

3.6. Effect of surfactant on NPs formation

In this section, PCL NPs were produced in a co-flow device at D_o = 200 μm and Q_{aq}/Q_{or} = 10 in the presence of four different types of hydrophilic surfactant, polyvinylpyrrolidone (PVP), polyvinyl alcohol (PVA), Tween 20 and Tween 80. The concentration of each surfactant in the aqueous phase was fixed at 1 wt%, which is a typical value in nanoprecipitation process (Xie and Smith, 2010). The minimum particle size of 387±7.0 nm was achieved using PVA, followed by PVP, Tween 20 and Tween 80. The Z_{ave} value for the NPs produced under the same conditions without any surfactant was 279±9 nm. The particle size was higher in the presence of surfactant in the aqueous phase which was due to the formation of surfactant layer on the particle surface. The presence of surfactant may also lead to an increase in the viscosity of aqueous phase which was reported to increase the particle size due to reduction in the rate of counter-diffusion of solvents (Tsukada et al., 2009).

3.7. Stability of NPs

The variation of the size of NPs with time is a good indicator of particle stability, since in most cases the particle size increases before macroscopic changes appear (Heurtault et al., 2003). In this study, the variations in mean particle size and zeta potential were measured over a storage period of 30 days at ambient temperature. Fig. 9 shows the average particle size, Z_{ave} and the zeta potential as a function of time for PCL NPs produced in a counter-flow device at D_o = 200 μm

and Q_{aq}/Q_{or} = 10 in the absence and presence of surfactant (PVP) in the aqueous phase. In the absence of any surfactant, the size of NPs increased from 244 to 486 nm, indicating that the presence of PVP in the aqueous phase was vital in order to improve the storage stability of NPs and prevent particle aggregation. In the presence of 1 wt% PVP, the initial particle size was higher, since each polymer particle was surrounded by the surfactant corona. Nevertheless, the Z_{ave} values increased only moderately over 30 days from 286 to 348 nm with negligible change in zeta potential from -3.72 to -3.37 mV. The same range of zeta potentials was reported by Filipović et al. (2013) for PCL-PVP NPs. The surfactant molecules are absorbed onto the surface of the newly formed PCL NPs with some chains extending away from the particle surface, which provides steric barrier and prevents particle coalescence (Lebouille et al., 2013).

3.8. Microscopic images of NPs

Scanning electron micrographs of PCL and PLA NPs are shown in Figs. 10 (a) and (b). The PLA particle exhibits a nearly perfect spherical shape, as reported by Lai and Tsiang (2004). The PCL particle is of a less regular shape and has a rougher surface morphology compared to the PLA NPs, due to crystallization of PCL on the surface (Lin and Huang, 2001). The surface of PLA NPs was very smooth because a fully amorphous poly-DL-lactide was used for particle formation. In addition, PCL NPs are larger than PLA NPs, which is in a good agreement with the dynamic light scattering data for the two polymers.

Figures 10 (c) and (d) are TEM images of PCL and PLA NPs. The PLA particles in Fig. 10 (d) have a very smooth surface and almost perfect spherical shape, as a result of surface energy minimization during their formation. The size of both NPs was within a range of 200-320 nm. When administrated intravenously, NPs should be sufficiently small (100-300 nm) to passively cross the tumor endothelial barrier and then retain in the tumor bed for prolonged time due to

reduced lymphatic drainage, which is known as the enhanced permeability and retention effect (Kobayashi et al., 2014). Particles larger than 1 μm are not convenient for intravascular delivery of drugs, since they can readily be opsonized with a possibility of capillary occlusion, while NPs smaller than 5 nm can be cleared rapidly from the blood via extravasation or renal clearance (Elsabahy and Wooley, 2012).

4. Conclusions

In this study, a new microfluidic method for the preparation of biodegradable nanoparticles was developed based on micromixing / nanoprecipitation in co-flow and flow focusing glass capillary devices. The particle size was precisely tuned by varying orifice size of the inner capillary, flow rate ratio and the total flow rate in the collection capillary. The higher the aqueous-to-organic flow rate ratio, the higher the dilution factor of the polymer in the liquid phase and the lower the rate of particle growth after nucleation, resulting in smaller particle size. At the same liquid flow rates, the mixing process was faster when the organic phase was injected through smaller orifice, which led to the generation of more nuclei, whose growth was limited by the amount of available polymer in the liquid phase, thereby resulting in smaller ultimate particle size. At constant flow rate ratio and orifice size, PLA formed smaller particles than PCL, because PLA is more compatible with water than PCL and starts to precipitate from a more diluted organic solution, which limits particle growth. The PLA particles exhibited a smoother surface and more regular spherical shape than PCL particles, which can be related to fully amorphous structure of D-L type polylactide.

In a co-flow device, a decrease in the aqueous-to-organic flow rate ratio led to the following sequential changes in the shape of the phase boundary: spherical interface → widening

jet → viscous fingering → vortex flow. A spherical interface suggests that a transient interfacial tension occurs between two miscible fluids (water and THF) immediately after injection as a result of high concentration gradients at the contact zone. In a flow focusing device, a widening-jet regime prevailed at all flow rates.

Smaller NPs were produced in a flow focusing device compared to a co-flow device of the same geometry, because in the former case the diameter of the organic stream was significantly smaller than the orifice diameter. PCL particles formed in flow focusing device with an orifice size of 200 μm at the organic stream flow rate of 1.7 mL h^{-1} and a flow rate ratio of 10 were smaller than 200 nm. Such small NPs are capable of spontaneous accumulations in various pathological sites via the enhanced permeability and retention effect. The mean size of PCL NPs formed in a co-flow device of the same geometry under the same flow rates was 227 nm.

The future work will be focused on encapsulation of hydrophobic drug (acetaminophen) within biodegradable polymer matrix and the optimization of process parameters using design of experiments (DOE) software and methods. The nanoparticles will be embedded with nanoclays to modify their internal structure and drug release patterns.

Acknowledgements

The authors gratefully acknowledge the financial support given for this work through the Ministry of Higher Education Malaysia. ZK Nagy would like to acknowledge financial support provided by the European Research Council grant no. [280106-CrySys].

References

Agrawal, A., Saran, A.D., Rath, S.S., & Khanna, A. (2004) Constrained nonlinear optimization for solubility parameters of poly(lactic acid) and poly(glycolic acid)−validation and comparison. *Polymer, 45*, 8603–8612.

Ali, H.S.M., York, P., & Blagden, N. (2009) Preparation of hydrocortisone nanosuspension through a bottom-up nanoprecipitation technique using microfluidic reactors. *International Journal of Pharmaceutics, 375*, 107–113.

Bagley, E.B., Nelson, T.P., & Scigliano, J.M. (1971). Three-dimensional solubility parameters and their relationship to internal pressure measurements in polar and hydrogen bonding solvents. *Journal of Paint Technology, 43*, 35−42.

Bilati, U., Allémann, E., & Doelker, E. (2005). Development of a nanoprecipitation method intended for the entrapment of hydrophilic drugs into nanoparticles. *European Journal of Pharmaceutical Sciences, 24*, 67−75.

Bordes, C., Fréville, V., Ruffin, E., Marote, P., Gauvrit, J. Y., Briançon, S., & Lantéri, P. (2010). Determination of poly(epsilon-caprolactone) solubility parameters: application to solvent substitution in a microencapsulation process. *International Journal of Pharmaceutics, 383*, 236−243.

British Standards Institution. (1997). Methods for determination of particle size distribution- Part 8: Photon correlation spectroscopy (p. BSI 11–1998).

Burrell, H. (1975). Solubility parameter values, In: Brandrup, J. & Immergut, E.H., Polymer Handbook. 2nd Ed. New York: J. Wiley & Sons, Inc., 337–359.

Capretto, L., Carugo, D., Mazzitelli, S., Nastruzzi, C., & Zhang, X. (2013). Microfluidic and lab-on-a-chip preparation routes for organic nanoparticles and vesicular systems for nanomedicine applications. *Advanced Drug Delivery Reviews, 65*, 1496−1532.

Choi, S.W., Kwon, H.Y., Kim, W.S., & Kim, J.H. (2002). Thermodynamic parameters on poly(D,L-lactide-co-glycolide) particle size in emulsification-diffusion process. *Colloids and Surfaces A: Physicochemical and Engineering Aspects, 201*, 283–289.

Dev, S., Prabhakaran, P., Filgueira, L., Iyer, K.S., & Raston, C.L. (2012). Microfluidic fabrication of cationic curcumin nanoparticles as an anti-cancer agent. *Nanoscale, 4*, 2575–2579.

Dev, S., Toster, J., Vadhan Prasanna, S., Fitzgerald, M., Swaminathan Iyer, K., & Raston, C.L. (2013). Suppressing regrowth of microfluidic generated drug nanocrystals using polyelectrolyte coatings. *RSC Advances, 3*, 695−698.

Douglas, S.J., Davis, S.S., & Illum, L. (1987). Nanoparticles in drug delivery. *Critical Reviews in Therapeutic Drug Carrier Systems, 3*, 233–261.

Elsabahy, M. & Wooley, K.L. (2012). Design of polymeric nanoparticles for biomedical delivery applications. *Chemical Society Reviews, 41*, 2545–2561.

Fessi, H., Devissaguet, J.P., Puisieux, F., & Thies, C. Process for the preparation of dispersible colloidal systems of a substance in the form of nanoparticles. US Patent 1992; 593–522.

Fessi, H., Puisieux, F., Devissaguet, J.P., Ammoury, N., & Benita, S. (1989). Nanocapsule formation by interfacial polymer deposition following solvent displacement. *International Journal of Pharmaceutics, 1989*, 55, R1−R4.

Filipović, N., Stevanović, M., Radulović, A., Pavlović, V., & Uskoković, D. (2013). Facile synthesis of poly(ε-caprolactone) micro and nanospheres using different types of

polyelectrolytes as stabilizers under ambient and elevated temperature. *Composites Part B: Engineering*, *45*, 1471−1479.

Galindo-Rodriguez, S., Allémann, E., Fessi, H., & Doelker, E. (2004). Physicochemical parameters associated with nanoparticle formation in the salting-out, emulsification-diffusion, and nanoprecipitation methods. *Pharmaceutical Research, 21*, 1428−1439.

Génot, V., Desportes, S., Croushore, C., Lefèvre, J.P., Pansu, R.B., Delaire, J.A., & von Rohr, P.R. (2010). Synthesis of organic nanoparticles in a 3D flow focusing microreactor. *Chemical Engineering Journal, 161*, 234−239.

Hansen C.M. Hansen Solubility Parameters: A User's Handbook. 2nd ed. Boca Raton: CRC Press; 2007.

Heurtault, B., Saulnier, P., Pech, B., Proust, J. E., & Benoit, J.P. (2003). Physico-chemical stability of colloidal lipid particles. *Biomaterials, 24*, 4283−4300.

Homsy, G.M. (1987). Viscous fingering in porous media. *Annual Review of Fluid Mechanics, 19*, 271−311.

Jahn, A., Stavis, S.M., Hong, J.S., Vreeland, W.N., DeVoe, D.L., & Gaitan, M. (2010). Microfluidic mixing and the formation of nanoscale lipid vesicles. *ACS Nano, 4*, 2077−2087.

Jain, R., Shah, N.H., Malick, A.W., & Rhodes, C.T. (1998). Controlled drug delivery by biodegradable poly(ester) devices: different preparative approaches. *Drug Development and Industrial Pharmacy, 24*, 703−727.

Jain, R.A. (2000). The manufacturing techniques of various drug loaded biodegradable poly(lactide-co-glycolide) (PLGA) devices. *Biomaterials, 21*, 2475−2490.

Jia, Z., & Liu, Z. (2013). Membrane-dispersion reactor in homogeneous liquid process. *Journal of Chemical Technology and Biotechnology, 88*, 163−168.

Joseph, D.D. & Hu, H.H. (1999). Interfacial tension between miscible liquids, in: Sachdev, P.L. & Venkatachalappa, M. (Eds.), Recent advances in fluid dynamics. CRC Press, Amsterdam, 137−156.

Karnik, R., Gu, F., Basto, P., Cannizzaro, C., Dean, L., Kyei-Manu, W., Langer, R., & Farokhzad, O.C. (2008). Microfluidic platform for controlled synthesis of polymeric nanoparticles. *Nano Letters, 8*, 2906–2912.

Khayata, N., Abdelwahed, W., Chehna, M.F., Charcosset, C., & Fessi, H. (2012). Stability study and lyophilization of vitamin E-loaded nanocapsules prepared by membrane contactor. *International Journal of Pharmaceutics, 439*, 254−259.

Kobayashi, K., Watanabe, R., & Choyke, P.L. (2014). Improving conventional enhanced permeability and retention (EPR) effects; What is the appropriate target? *Theranostics*, *4*, 81-89.

Lai, M.K. & Tsiang, R.C. (2004). Encapsulating acetaminophen into poly(L-lactide) microcapsules by solvent-evaporation technique in an O/W emulsion. *Journal of Microencapsulation, 21*, 307−316.

Laouini, A., Charcosset, C., Fessi, H., Holdich, R.G., & Vladisavljević, G.T. (2013a). Preparation of liposomes: a novel application of microengineered membranes − investigation of the process parameters and application to the encapsulation of vitamin E3. *RSC Advances, 3*, 4985–4994.

Laouini, A., Charcosset, C., Fessi, H., Holdich, R.G., & Vladisavljević, G.T. (2013b). Preparation of liposomes: a novel application of microengineered membranes: From laboratory scale to large scale. *Colloids and Surfaces B: Biointerfaces 112*, 272–278.

Laouini, A., Koutroumanis, K.P., Charcosset, C., Georgiadou, S., Fessi, H., Holdich, R.G., & Vladisavljević, G.T. (2013c). pH-Sensitive micelles for targeted drug delivery prepared using a novel membrane contactor method. *ACS Applied Materials and Interfaces 5*, 8939–8947.

Lebouille, J.G.J.L., Stepanyan, R., Slot, J.J.M., Cohen Stuart, M.A., & Tuinier, R. (2013). Nanoprecipitation of polymers in a bad solvent. *Colloids and Surfaces A: Physicochemical and Engineering Aspects*, *460*, 225−235.

Legrand, P., Lesieur, S., Bochot, A., Gref, R., Raatjes, W., Barratt, G., & Vauthier, C. (2007). Influence of polymer behaviour in organic solution on the production of polylactide nanoparticles by nanoprecipitation. *International Journal of Pharmaceutics, 344*, 33–43.

Lin, W.J. & Huang, L.I. (2001). Influence of pluronics on protein-loaded poly(ε-caprolactone) microparticles. *Journal of Microencapsulation*, *18*, 191–197.

Lince, F., Marchisio, D.L., & Barresi, A.A. (2008). Strategies to control the particle size distribution of poly-ε-caprolactone nanoparticles for pharmaceutical applications. *Journal of Colloid and Interface Science, 322*, 505–515.

Lu, Y. & Chen, S.C. (2004). Micro and nano-fabrication of biodegradable polymers for drug delivery. *Advanced Drug Delivery Reviews*, *56*, 1621−1633

Martin, A., Bustamante, P., Chun, A.H.C. Physical Pharmacy, 4th Ed., Lea & Febiger, Philadelphia, U.S.A. (1993). 556−594.

Mohanraj, V.J. & Chen, Y. (2007). Nanoparticles − A review. *Tropical Journal of Pharmaceutical Research, 5*, 561−573.

Nagavarma, B.V.N., Hemant, K.S.Y., Ayaz, A., Vasudha, L.S., & Shivakumar, H. G. (2012). Different techniques for preparation of polymeric nanoparticles - A review. *Asian Journal of Pharmacology, 5*, 16–23.

Panyam, J. & Labhasetwar, V. (2003). Biodegradable nanoparticles for drug and gene delivery to cells and tissue. *Advanced Drug Delivery Reviews, 55*, 329–347.

Rao, J. & Geckeler, K. (2011). Polymer nanoparticles: preparation techniques and size-control parameters. *Progress in Polymer Science, 36*, 887–913.

Södergård, A. & Stolt, M. (2002). Properties of lactic acid based polymers and their correlation with composition. *Progress in Polymer Science, 27*, 1123−1163.

Soppimath, K.S., Aminabhavi, T.M., Kulkarni, A.R., & Rudzinski, W.E. (2001). Biodegradable polymeric nanoparticles as drug delivery devices. *Journal of Controlled Release, 70*, 1–20.

Su, Y.F., Kim, H., Kovenklioglu, S., & Lee, W.Y. (2007). Continuous nanoparticle production by microfluidic-based emulsion, mixing and crystallization. *Journal of Solid State Chemistry, 180*, 2625–2629.

Submicron, D.N. (2011). User's Manual: Delsa^{TM} Nano Subricon Particle Size and Zeta Potential. Beckman Coulter Ireland Inc.

Tsukada, Y., Hara, K., Bando, Y., Huang, C.C., Kousaka, Y., Kawashima, Y., et al. (2009). Particle size control of poly(dl-lactide-co-glycolide) nanospheres for sterile applications. *International Journal of Pharmaceutics, 370*, 196–201.

Van Krevelen, D.W. & Hoftyzer, P.J. (1976). Properties of Polymers: Their Estimation and Correlation with Chemical Structure. 2nd Ed. Amsterdam-Oxford-New York: Elsevier Scientific Publishing Company.

Vladisavljević, G.T., Duncanson, W.J., Shum, H.C., & Weitz, D.A. (2012). Emulsion templating of poly(lactic acid) particles: droplet formation behaviour. *Langmuir 28*, 12948–12954.

Vladisavljević, G.T., Laouini, A., Charcosset, C., Fessi, H., Bandulasena, H.C.H., & Holdich, R.G. (2014). Production of liposomes using microengineered membrane and co-flow microfluidic device. *Colloids and Surfaces A: Physicochemical and Engineering Aspects*, *458*, 168–177.

Xie, H. & Smith, J.W. (2010). Fabrication of PLGA nanoparticles with a fluidic nanoprecipitation system. *Journal of Nanobiotechnology*, *8*, 1–18.

Yun, J., Zhang, S., Shen, S., Chen, Z., Yao, K., & Chen, J. (2009). Continuous production of solid lipid nanoparticles by liquid flow-focusing and gas displacing method in microchannels. *Chemical Engineering Science*, *64*, 4115–4122.

Zhang, S., Yun, J., Shen, S., Chen, Z., Yao, K., Chen, J., & Chen, B. (2008). Formation of solid lipid nanoparticles in a microchannel system with a cross-shaped junction. *Chemical Engineering Science*, *63*, 5600–5605.

Zhao, H., Wang, J.X., Wang, Q.A., Chen, J.F., & Yun, J. (2007). Controlled liquid antisolvent precipitation of hydrophobic pharmaceutical nanoparticles in a microchannel reactor. *Industrial and Engineering Chemistry Research*, *46*, 8229–8235.

Figure 1
Click here to download Figure: Figure 1.docx

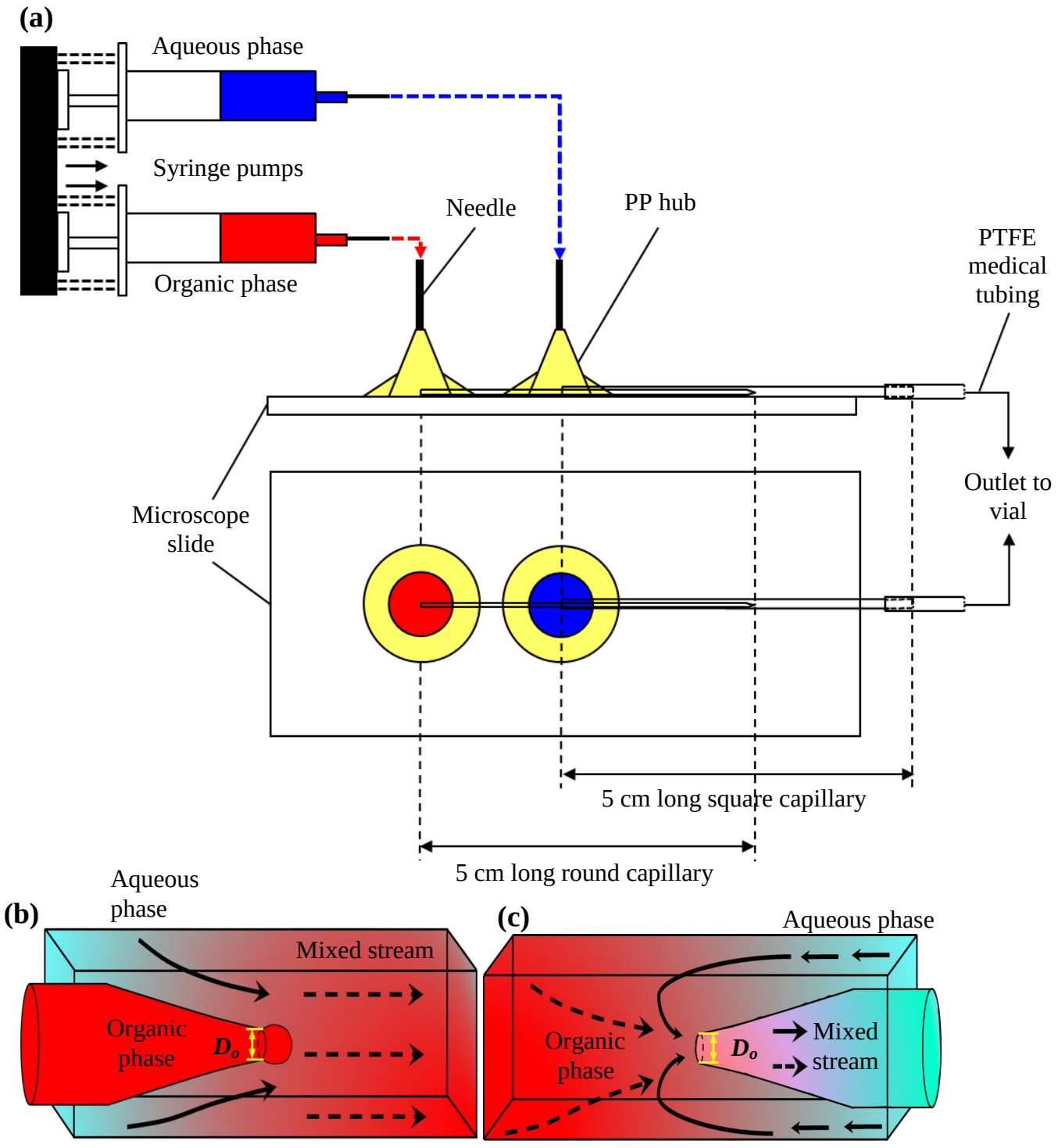

Fig. 1. (a) A schematic of the experimental set-up with a co-flow glass capillary device: (top) side view, (bottom) bird's-eye view; (b-c) Magnified views of a region near the orifice for: (b) co-flow; (c) flow focusing (c). D_o = orifice diameter.

Figure 2
Click here to download Figure: Figure 2.docx

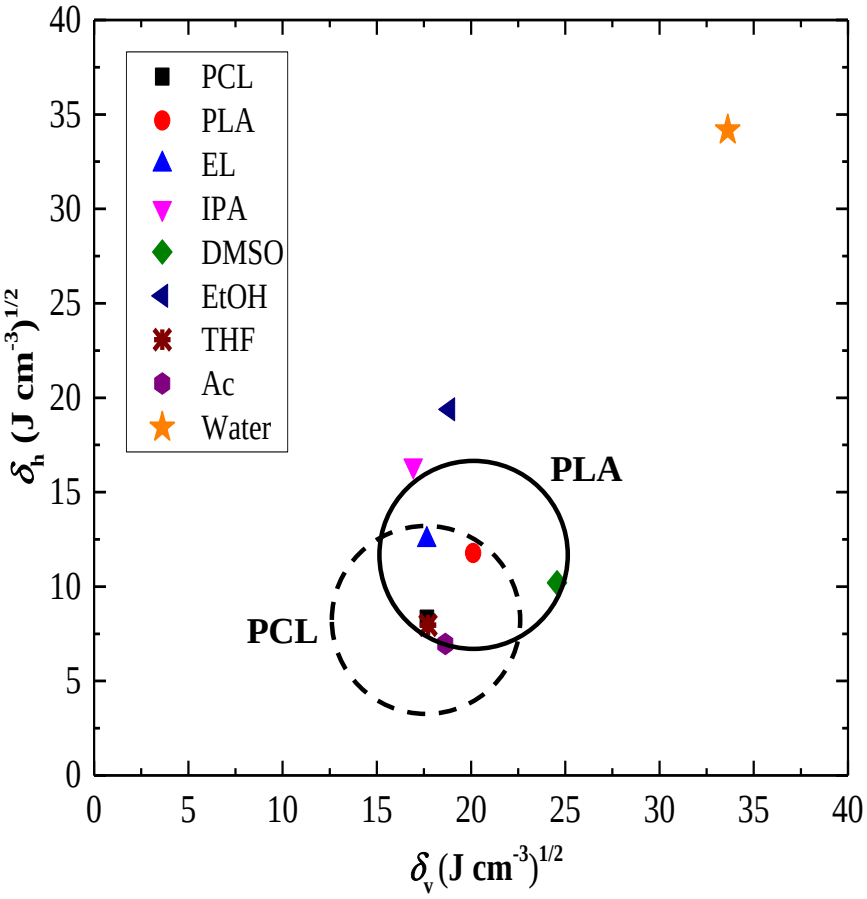

Fig. 2. Bagley's two-dimensional graph of the partial solubility parameters of the solvents with respect to the partial solubility parameters determined for PLA and PCL.
(line **--** = solubility circle limit for PCL; line **—** = solubility circle limit for PLA).

Figure 3
Click here to download Figure: Figure 3.docx

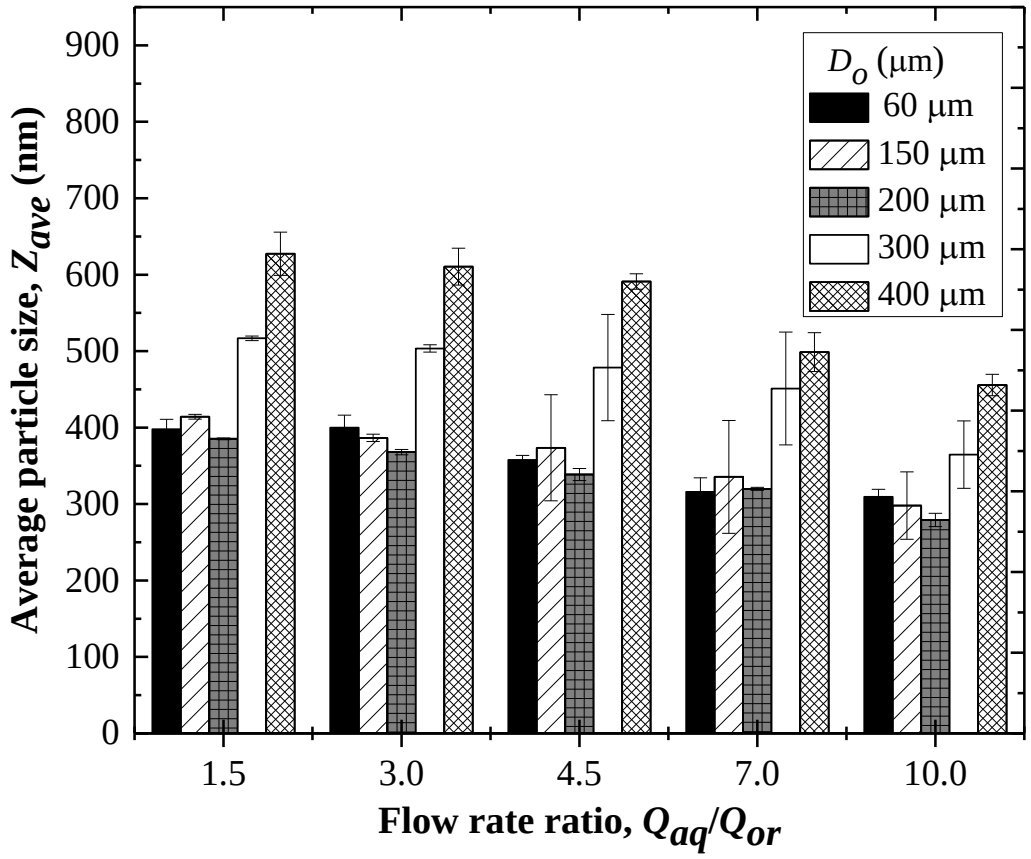

Fig. 3. The average size, Z_{ave} of PCL nanoparticles produced in a co-flow device at Q_{aq}=5 ml h^{-1} as a function of flow rate ratio, Q_{aq}/Q_{or} and orifice diameter, D_o. The organic phase was 1 g L^{-1} PCL in THF and the aqueous phase was Milli-Q water.

Figure 4
Click here to download Figure: Figure 4.docx

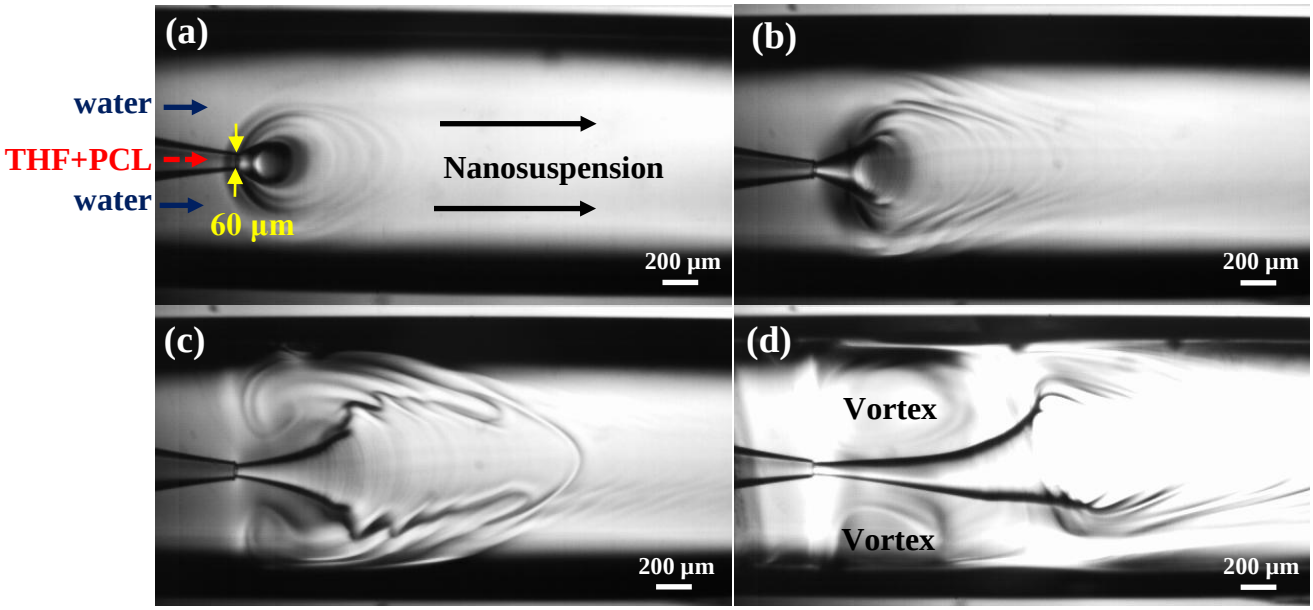

Fig. 4. The shape of liquid/liquid interface in a co-flow device with a 60-µm orifice diameter at Q_{aq}=5 ml h^{-1} and a flow rate ratio, Q_{aq}/Q_{or} of: (a) 10.0; (b) 4.5; (c) 3.0; (d) 1.5. The organic phase was 1 g L^{-1} PCL in THF and the aqueous phase was Milli-Q water.

Figure 5
Click here to download Figure: Figure 5.docx

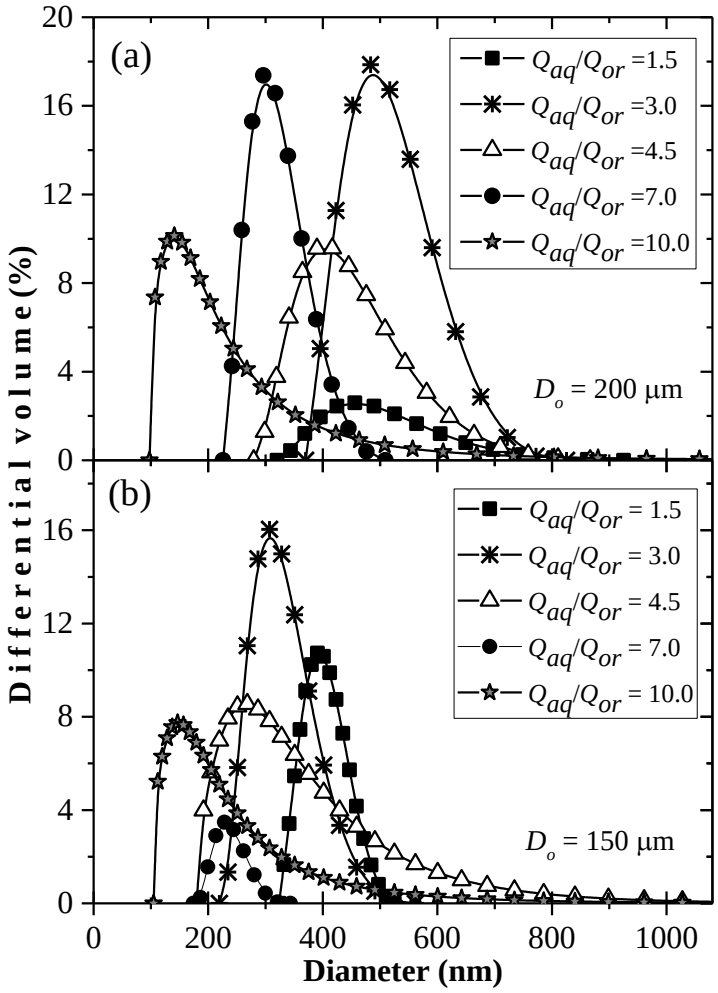

Fig. 5. The size distribution of PCL NPs as a function of aqueous-to-organic flow rate ratio in a co-flow device at Q_{aq} =5 ml h^{-1}. The orifice size, D_o : (a) 200 µm; (b) 150 µm. The organic phase was 1 g L^{-1} PCL in THF and the aqueous phase was Milli-Q water.

Figure 6
Click here to download Figure: Figure 6.docx

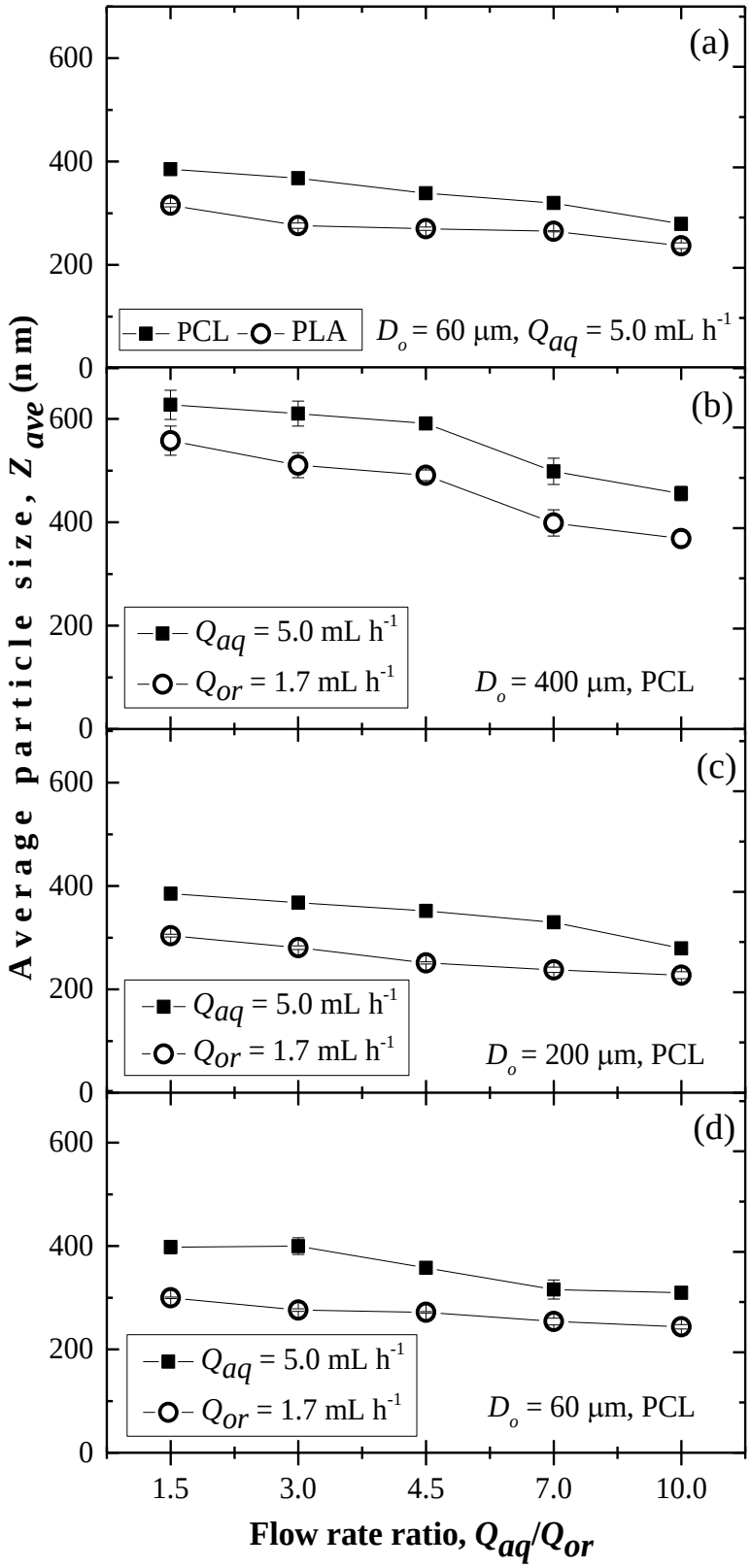

Fig. 6. The average particle size, Z_{ave} as a function of flow rate ratio, Q_{aq}/Q_{or} and orifice diameter, D_o in a co-flow device. The flow rate of either organic or aqueous phase was kept constant in each series of experiments. The organic phase was 1 g L^{-1} PCL or PLA in THF (Figure a) or 1 g L^{-1} PCL in THF (Figures b to d) and the aqueous phase was Milli-Q water.

Figure 7
Click here to download Figure: Figure 7.docx

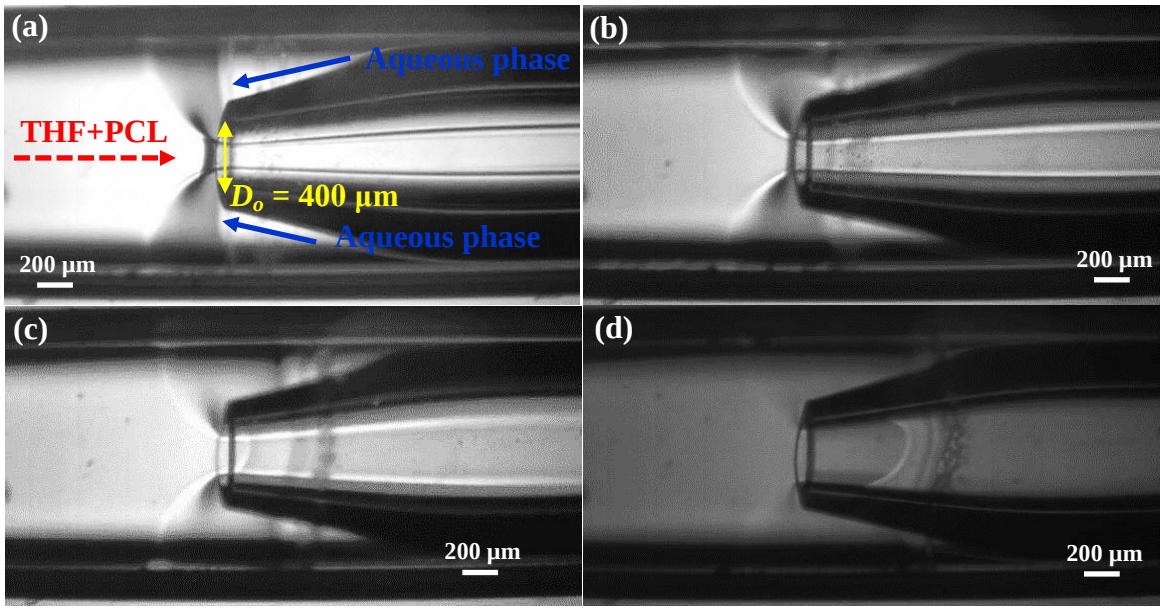

Fig. 7. The shape of liquid/liquid interface in a counter-counter flow device with a 400-µm orifice diameter at Q_{or} = 1.7 ml h^{-1} and Q_{aq}/Q_{or} of: (a) 10.0; (b) 7.0; (c) 4.5; and (d) 3.0. The organic phase was 1 g L^{-1} PCL in THF and the aqueous phase was Milli-Q water.

Figure 8
Click here to download Figure: Figure 8.docx

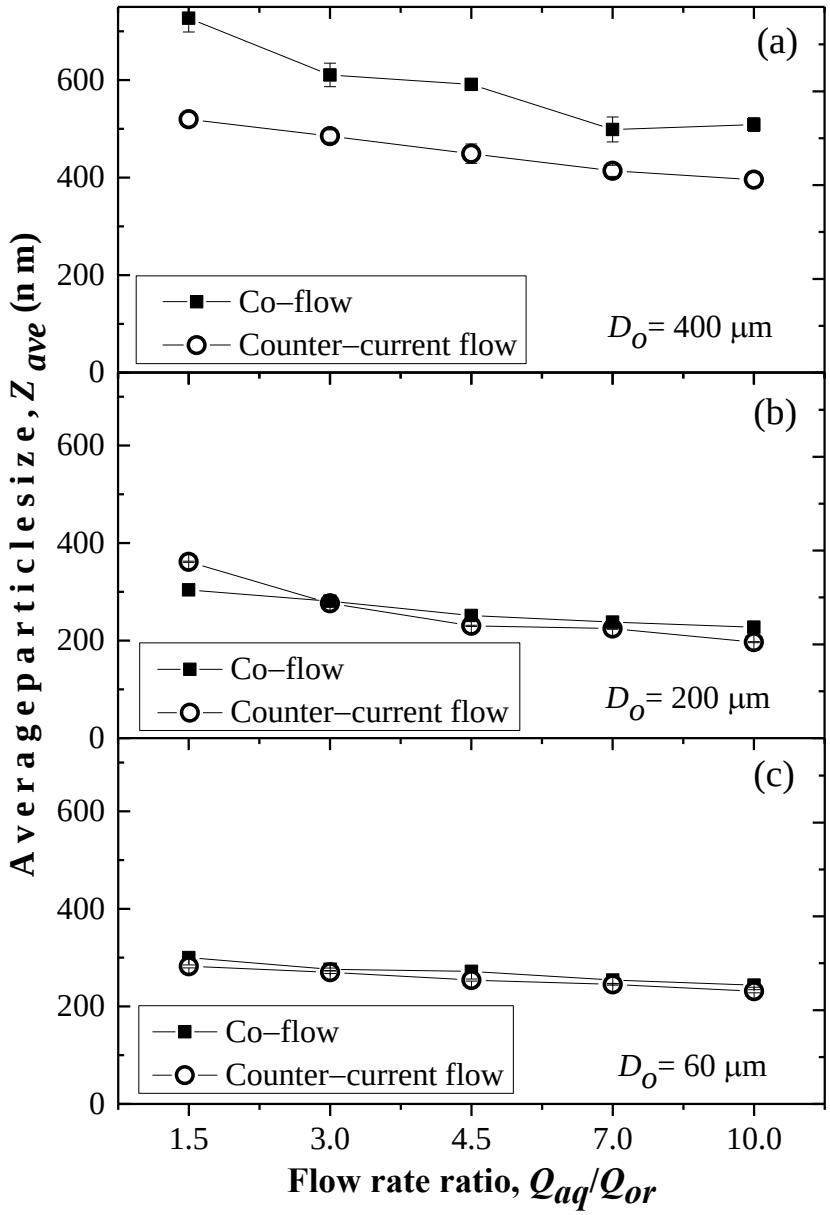

Fig. 8. (a) The comparison of average particle size, Z_{ave} in a co-current and counter-current flow device at Q_{or} = 1.7 mL h^{-1} for the orifice diameter, D_o of: (a): 400 µm; (b) 200 µm; (c) 60 µm. The organic phase was 1 g L^{-1} PCL in THF and the aqueous phase was Milli-Q water.

Figure 9
Click here to download Figure: Figure 9.docx

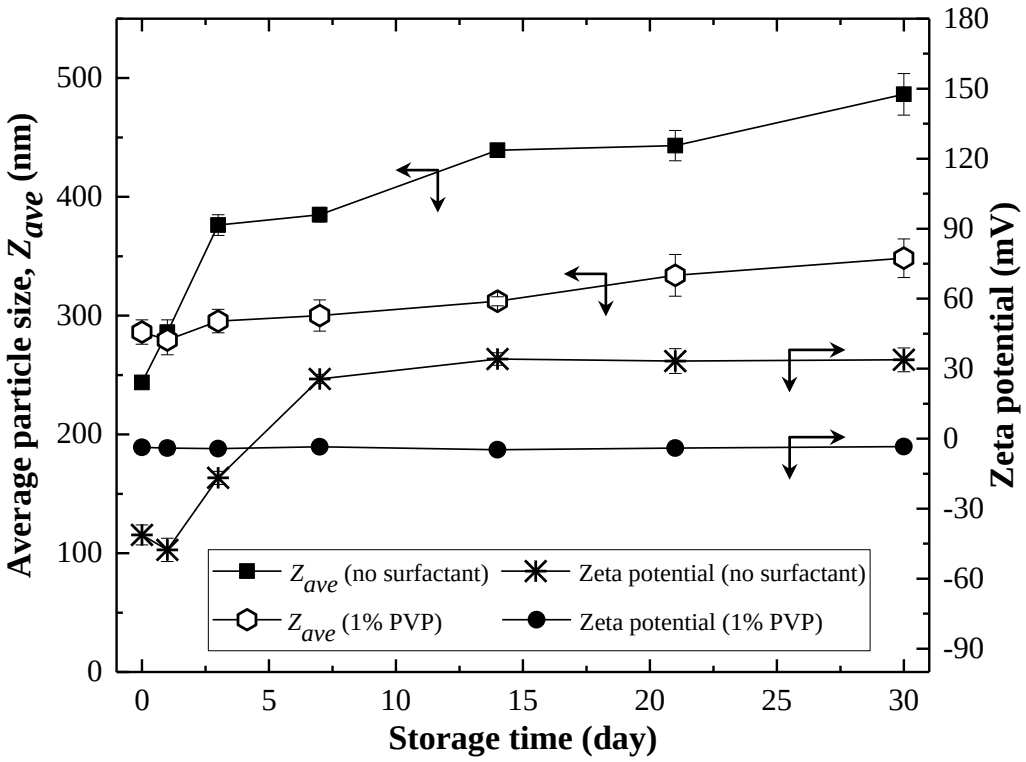

Fig. 9. The average size, Z_{ave}, and zeta-potential of PCL NPs over a 30 day storage period at atmospheric pressure and ambient temperature. The particles were produced in a counter-current flow device at Q_{aq}/Q_{or}=10, Q_{or}= 1.7 mL h^{-1}, and D_o =200 μm. The organic phase was 1 g L^{-1} PCL in THF and the aqueous phase was Milli-Q water or 1 wt% PVP.

Figure 10
Click here to download Figure: Figure 10.docx

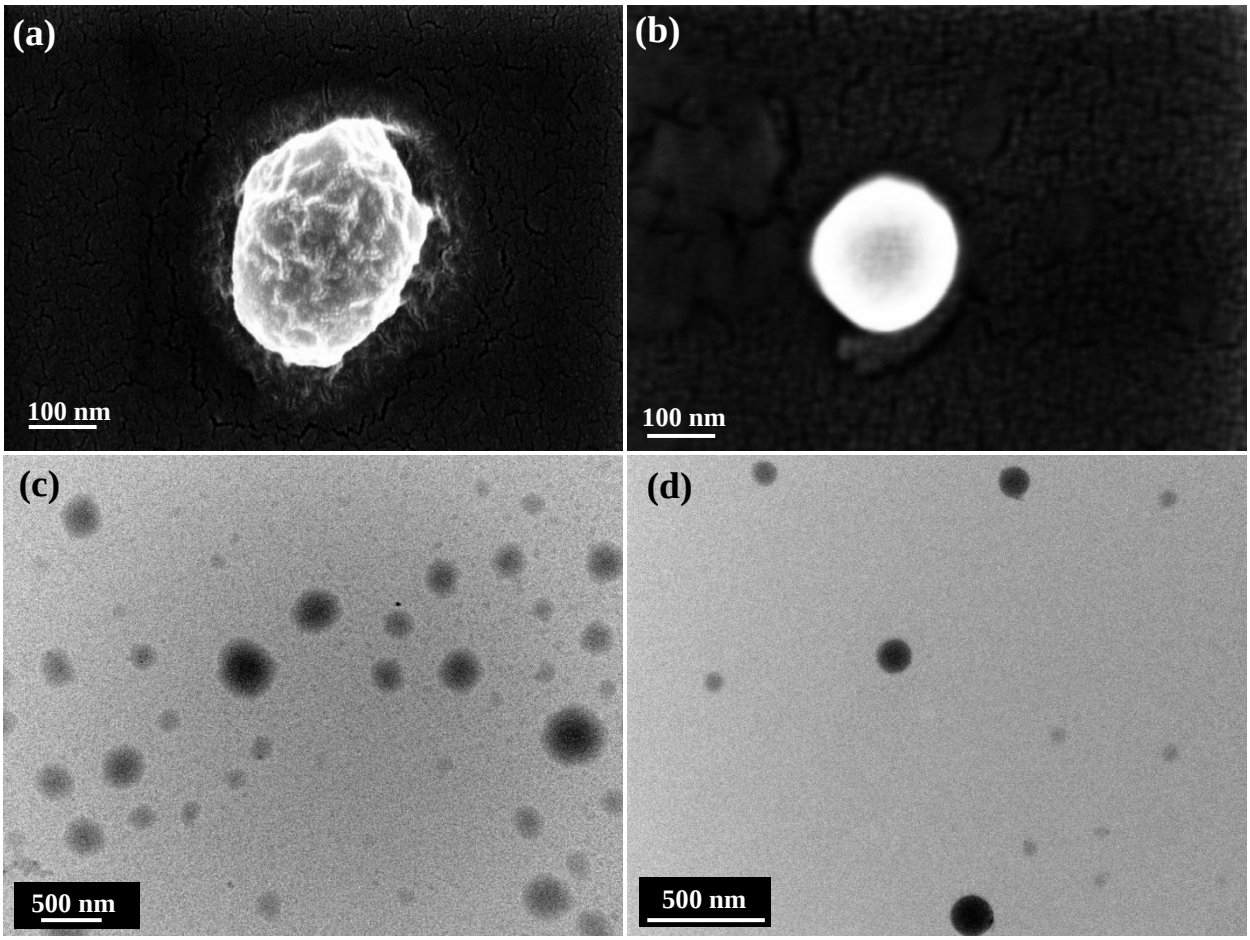

Fig. 10. (a) FEG-SEM micrograph of individual PCL particle; (b) FEG-SEM micrograph of individual PLA particle; (c) TEM image of PCL NPs; (d) TEM image of PLA NPs.

Table 1

The partial solubility parameters, δ_d, δ_p, δ_h, and δ_v, and the total solubility parameters, δ_t, of different solvents and polymers, the combined solubility parameters, $\Delta\delta_{solvent-water}$ and $\Delta\delta_{polymer-water}$, and the interaction parameters, $\chi_{solvent-water}$ and $\chi_{polymer-water}$ (Ac = acetone, THF = tetrahydrofuran, EtOH = ethanol, DMSO = dimethyl sulfoxide, IPA = isopropyl alcohol, EL = ethyl lactate, PLA = polylactide, PCL = poly-ε-caprolactone).

Solubility parameters $(J\ cm^{-3})^{1/2}$	Water	Ac	THF	EtOH	DMSO	IPA	EL	PLA[a]	PLA[b]	PCL[c]
$\delta_d = \Sigma F_{di} / V$	12.28	15.46	16.77	15.77	18.36	15.80	15.95	17.62	18.50	17.00
$\delta_p = (\Sigma F_{pi}^2)^{1/2} / V$	31.30	10.40	5.71	10.32	16.32	6.10	7.57	9.70	9.70	4.80
$\delta_h = (\Sigma E_{hi} / V)^{1/2}$	34.17	6.96	7.96	19.38	10.20	16.40	12.48	11.77	6.00	8.30
$\delta_v = (\delta_p^2 + \delta_d^2)^{1/2}$	33.62	18.64	17.72	18.85	24.56	16.94	17.66	20.11	20.89	17.66
$\delta_t = (\delta_p^2 + \delta_d^2 + \delta_h^2)^{1/2}$	48.08	19.90	19.42	27.03	26.60	23.58	21.62	23.31	21.73	19.52
$\Delta\delta_{solvent-water}$ or $\Delta\delta_{polymer-water}$	0.00	34.45	36.91	25.91	28.91	31.04	32.36	31.57	36.04	37.33
$\chi_{solvent-water}$ or $\chi_{polymer-water}$	0.00	23.93	27.33	10.61	13.45	18.84	32.94	6.85	6.46	7.13

The partial solubility parameters of the solvents were taken from Burrell (1975). δ, solubility parameter; subscripts: *t*, total; *d*, contribution of the dispersion forces; *p*, polar contribution; *h*, hydrogen bonding contribution; *v*, dispersion and polar contribution. *V*, molar volume of the compound; *i*, structural groups within the molecule; F_{di} and F_{pi}, molar attraction constants due to dispersion and polar interactions, respectively; E_{hi}, energy of hydrogen bonding.

a The partial solubility parameters of PLA calculated using the classical method of Van Krevelen and Hoftyzer (1976).

b The partial solubility parameters of PLA calculated using the constrained nonlinear optimization method of Agrawal et al. (2004).

c The partial solubility parameters of PCL calculated using the classical method of Van Krevelen and Hoftyzer (1976).

Table 2

The distance D between a solvent (*S*) and the solute (*P*) in the "$2\delta_d$ - δ_p - δ_h" space and the interaction radius, R_0. The points located outside of the solubility circle for the polymer are bolded. Abbreviations and superscripts have the same meaning as in Table 1.

	Ac	THF	EtOH	DMSO	IPA	EL	R_0
$D_{PLA^a-solvent}$	**6.50**	5.77	**8.49**	**6.96**	**6.90**	4.02	6.4
$D_{PLA^b-solvent}$	6.19	5.63	**14.47**	7.84	**12.26**	8.52	10.5
$D_{PCL-solvent}$	6.53	1.08	**12.62**	**11.99**	**8.55**	5.44	7.1

Table 3

The combined polymer-solvent solubility parameters, $\delta_{polymer\text{-}solvent}$ and the polymer-solvent interaction parameters, $\chi_{polymer\text{-}solvent}$. Abbreviations and superscripts have the same meaning as in Table 1. The values of $\chi_{solvent-polymer} < 0.5$ are bolded indicating a good solvent for the polymer.

Solvent	$\Delta\delta_{polymer-solvent}$ (J cm^{-3})$^{1/2}$			$\chi_{solvent-polymer}$		
	PLA[a]	PLA[b]	PCL[c]	PLA[a]	PLA[b]	PCL[c]
Ac	5.32	3.26	5.96	0.85	**0.32**	1.07
THF	5.58	4.77	1.00	1.04	0.76	**0.03**
EtOH	7.86	13.67	12.44	1.48	4.48	3.71
DMSO	6.84	7.84	11.75	1.36	1.79	4.03
IPA	6.14	11.33	8.29	1.18	4.03	2.16
EL	2.80	7.28	5.12	**0.37**	2.50	1.24

Table 4

The average size, Z_{ave} and polydispersity index, PDI of NPs before and after solvent removal and the resultant linear and volumetric particle size reduction as a function of orifice diameter in a co-flow device at $Q_{aq}/Q_{or} = 10$ ($Q_{aq} = 5$ mL h^{-1}, $Q_{or} = 0.5$ mL h^{-1}). The organic phase was 1 g L^{-1} PCL in THF and the aqueous phase was Milli-Q water.

Orifice diameter (μm)	Without solvent removal		With solvent removal		Linear size reduction (%)	Volume reduction (%)
	Z_{ave} (nm)	PDI	Z_{ave} (nm)	PDI		
60	359 ± 52	0.210 ± 0.016	309 ± 46	0.219 ± 0.010	14	36
150	471 ± 43	0.215 ± 0.008	418 ± 24	0.242 ± 0.014	11	30
200	319 ± 14	0.178 ± 0.057	279 ± 9	0.237 ± 0.060	13	33
300	396 ± 69	0.190 ± 0.008	355 ± 44	0.249 ± 0.025	10	28
400	594 ± 25	0.219 ± 0.008	509 ± 14	0.297 ± 0.050	14	37

Video 1 Caption

Click here to download Supplementary Material: Video 1 caption.docx

Video 1

Click here to download Supplementary Material: Video 1.mp4